



Science Arts & Métiers (SAM)

is an open access repository that collects the work of Arts et Métiers Institute of Technology researchers and makes it freely available over the web where possible.

This is an author-deposited version published in: <https://sam.ensam.eu>
Handle ID: <http://hdl.handle.net/10985/13775>

To cite this version :

Nazih MECHBAL, Marc RÉBILLAT - Damage localization in composite plates using canonical polyadic decomposition of Lamb wave difference signals tensor - In: 9th European Workshop on Structural Health Monitoring, Royaume-Uni, 2018-07 - 9th European Workshop on Structural Health Monitoring - 2018

Any correspondence concerning this service should be sent to the repository

Administrator : scienceouverte@ensam.eu



Damage localization in composite plates using canonical polyadic decomposition of Lamb wave difference signals tensor

Marc Rebillat¹ and Nazih Mechbal¹

*1 PIMM Laboratory, ENSAM, CNRS, CNAM, Hesam Université, Paris, France
(e-mail: marc.rebillat@ensam.eu – nazih.mechbal@ensam.eu)*

Abstract

Monitoring in real-time and autonomously the health state of aeronautic structures is referred to as Structural Health Monitoring (SHM) and is a process decomposed in four steps: damage detection, localization, classification, and quantification. The structure under study is here a complex aeronautic nacelle and the focus is put on the localization step of the SHM process. The fact that SHM data are naturally three-way tensors is here investigated for this purpose. It is demonstrated that under classical assumptions regarding wave propagation, the canonical polyadic decomposition of rank 2 of the tensor built from the phase of the difference signals between a healthy and damaged states provides direct access to the distances between the piezoelectric elements and the damage. This property is used here to propose an original and robust tensor-based damage localization algorithm. This algorithm is successfully validated on experimental data coming from the aeronautic nacelle equipped with 30 mounted piezoelectric elements.

1. Introduction

Monitoring in real-time and autonomously the health state of structures is of high interest in the industry, and more specifically in the aeronautic and civil engineering applications fields. Such a process is referred to as Structural Health Monitoring (SHM) [1, 2]. To achieve this goal, structures become “*smart*” in the sense that they are equipped with sensors, actuators, and artificial intelligence that allow them to state autonomously regarding their own health. One can compare smart structures with the human body which, thanks to its various senses and nerves, is able to assess if it has been hurt, where it has been hurt, and to estimate how severe it is. Following this analogy, the SHM process is classically decomposed into four steps: damage detection, localization, classification, and quantification [3].

The structure under study is here a composite complex aeronautic nacelle excited by means of Lamb waves. To deploy SHM to such structure, it is equipped with piezoelectric elements that can be used both as sensors and actuators. Each element is actuated one by one using a tone burst at high frequency, produces a Lamb wave that propagates throughout the structure, and the resulting Lamb wave is finally measured by the other piezoelectric elements acting as sensors. If a structure equipped with N piezoelectric elements and for which acquisition is performed over K samples is considered, one naturally ends up with a tensor $\mathbf{M} \in \mathbb{R}^{N \times N \times K}$ at the end of the SHM process. To monitor the possible apparition of damage, measurements are first performed in a reference state to get a reference tensor \mathbf{R} . Then, during the life cycle of the structure measurements at unknown states are performed and provides the tensor \mathbf{U} . The tensor $\mathbf{\delta}$ that corresponds to the difference between \mathbf{R} and \mathbf{U} is the basis of the detection, localization, classification, and quantification steps of SHM.

The three-dimensional nature of the difference tensor $\mathbf{\delta} \in \mathbb{R}^{N \times N \times K}$ allows for the use of specific analysis tools [4, 5, 6]. Even if during the last decade, tensors analysis have been widely applied for signal processing purposes [4, 5, 6], they have found relatively

few applications in SHM and reported applications mainly focused on the detection step. For example: damage detection based on tensors in a civil engineering context [7, 8], tensor-based damage detection for non-destructive evaluation of composite structures using ultrasounds [9], or application of tensors for denoising purposes in composite plates monitored by ultrasonic waves [10]. Thus, to the knowledge of the authors, the advantages of tensors for damage localization by means of Lamb waves in composite plates has never been investigated.

The focus is thus put in this paper on the localization step of the SHM process. Classical methods for damage localization by means of Lamb waves in composite plates are usually based on a path by path analysis of data [11, 12, 13] (*i.e.* on only one row of the tensor $\delta \in \mathbb{R}^{N \times N \times K}$). Typically, the time-of-flight for each path “*actuator-sensor*” is extracted, and then using knowledge of the wave propagation speed and by means of triangulation the damage localization is estimated [11, 12, 13]. These methods thus process each path independently and then integrate all the information together to form a localization map from which damage localization is inferred. As SHM data are three-way, highly redundant, and correlated, a vector-based one-way approach as depicted above cannot capture all these relationships and correlations together. The tensors thus appear as a very promising tool able to improve damage localization by means of Lamb waves in composite plates. The paper is organized as follows: a tensor-based damage localization algorithm is detailed in Section 2 and then validated experimentally in Section 3. A conclusion and a discussion are then drawn in Section 4.

2. Tensor based damage localization

2.1. A simple physical model of Lamb wave propagation

Wave propagation within structures can be as a first approximation thought as a very simple physical phenomenon: waves propagate with a velocity v in all directions around their excitation point and are attenuated with an attenuation factor $\alpha(d) \in \mathbb{R}^+$ that is distance dependent. Then, in the absence of damage, a wave $s(t)$ is sent by the piezoelectric element n and the elements $\{m \in 1:N, m \neq n\}$ receives the signals:

$$s_{nm}^R(t) = \alpha(d_{nm})s\left(t - \frac{d_{nm}f_s}{v}\right) \quad \text{Eq. 1}$$

where d_{nm} denotes the distance between the elements n and m , t the sampled time and f_s the sampling frequency. It is important to notice here that isotropy is assumed whereas it may not be perfectly the case in practice.

Let’s now introduce a damage at position D within this structure. When the wave emitted by the element n hit the damage, it is reflected, and a new wave is reemitted within the structure. As a first approximation, one can assume that damage acts as a secondary wave source that reemits any incoming wave in all directions with a reflection coefficient $\beta \in \mathbb{R}^+$. The signal received by the element m is then:

$$s_{nm}^U(t) = s_{nm}^R(t) + \beta\alpha(d_{nD})\alpha(d_{Dm})s\left(t - \frac{f_s(d_{nD} + d_{Dm})}{v}\right) \quad \text{Eq. 2}$$

If the focus is now put on the difference signal, one has:

$$\delta_{nm}(t) = s_{nm}^U(t) - s_{nm}^R(t) = \beta\alpha(d_{nD})\alpha(d_{Dm})s\left(t - \frac{f_s(d_{nD} + d_{Dm})}{v}\right) \quad \text{Eq. 3}$$

It is then possible to take the Fourier transform of this signal and one ends up with the following transfer function:

$$H_{nmk} = \frac{\Delta_{nm}(k - k_0)}{S(k - k_0)} = \beta \alpha(d_{nD}) \alpha(d_{Dm}) \exp \left(-i 2\pi f_s (k - k_0) \left(\frac{d_{nD} + d_{Dm}}{Kv} \right) \right) \quad \text{Eq. 4}$$

where $S(k - k_0)$ denotes the Fourier transform of the input signal $s(t)$, $\Delta_{nm}(k - k_0)$ the Fourier transform of the difference signal $\delta_{nm}(t)$, and K the total number of samples. k_0 and k_M stands for the frequency indexes over which the phase analysis starts and stops. H_{nmk} is thus the k -th coefficient of the Fourier transform for the difference signal on the path “actuator n – sensor m ” It is then possible to compute the phase of each element:

$$\Phi_{nmk} = \phi[H_{nmk}] = -2\pi f_s (k - k_0) \left(\frac{d_{nD} + d_{Dm}}{Kv} \right) \quad \text{Eq. 5}$$

The tensor $\Phi \in \mathbb{R}^{N \times N \times K}$ containing the coefficients Φ_{nmk} can be interpreted as a three-way tensor [4, 5, 6].

2.2. Canonical polyadic decomposition of the phase tensor

The idea is now to be able to make a structure popping out of the tensor Φ defined in Eq. 5. From tensors literature, it is well known that tensors can be decomposed using the Canonical Polyadic Decomposition (CPD) up to a rank R [4, 5, 6]. Such a decomposition consists in finding a triplet $(\mathbf{a} \in \mathbb{R}^{N \times R}, \mathbf{b} \in \mathbb{R}^{N \times R}, \mathbf{c} \in \mathbb{R}^{K \times R})$ that allows for a more compact representation of a given tensor (see Fig. 1).

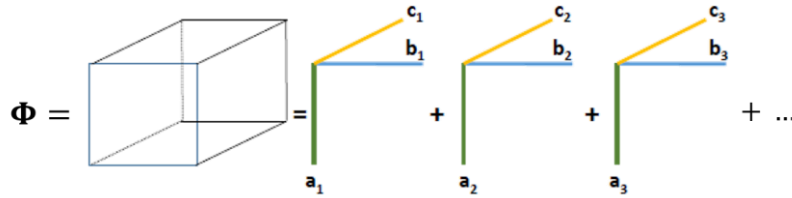


Fig. 1: Schematic representation of the CPD of the tensor Φ

According to the notations of Fig. 1, the CPD of the phase tensor Φ defined in Eq. 5 can be expressed as:

$$\Phi_{nmk} = - \sum_{r=1}^R a_{nr} b_{mr} c_{kr} \quad \text{Eq. 6}$$

What is interesting here is that by analyzing Eq. 5 and by exploiting the fact that $\forall i \in [1, N] d_{iD} = d_{Di}$, the tensor Φ can be exactly expressed as a tensor of rank $R = 2$ by choosing:

$$\mathbf{a} = \begin{bmatrix} d_{1D} & 1 \\ \dots & \dots \\ d_{ND} & 1 \end{bmatrix} \quad \mathbf{b} = \begin{bmatrix} 1 & d_{1D} \\ \dots & \dots \\ 1 & d_{ND} \end{bmatrix} \quad \mathbf{c} = \frac{2\pi f_s}{Kv} \begin{bmatrix} (k_0 - k_0) & (k_0 - k_0) \\ \dots & \dots \\ (k_M - k_0) & (k_M - k_0) \end{bmatrix} \quad \text{Eq. 7}$$

By looking in more detail at this tensor decomposition, it is particularly striking to notice that \mathbf{a} and \mathbf{b} both theoretically provide direct access to $\{d_{iD}\}_{i \in [1, N]}$ that are the distances between each piezoelectric element and the damage position. On the knowledge of these distances, damage localization is thus theoretically possible. Furthermore, \mathbf{c} is parametrized by v the wave velocity within the material and by the signal processing parameters f_s and K and is thus relatively easy to estimate.

In summary, it is demonstrated that the CPD of rank $R = 2$ of the phase of the difference signals between a healthy and damaged states potentially provides direct access to all the distances between the piezoelectric elements and the damage, which could allow for damage localization.

2.3. Managing unicity of CPD

Unfortunately, even if very efficient numerical tools are available to compute a CPD for a given tensor [14], such a decomposition is not unique. The issue is that here not only a decomposition is sought, but a decomposition that can be physically interpreted according to Eq. 7. It is however possible here to exploit the powerful property that the CPD is unique up to a scaling and a permutation of its terms. This guarantees that a decomposition of arbitrary choice can always be found. Therefore, a meaningful way to descale a numerically obtained CPD, or to obtain a unique one that makes sense physically is needed.

Mathematically, for the phase tensor Φ , once a first decomposition $(\mathbf{a}, \mathbf{b}, \mathbf{c})$ has been numerically obtained, what is needed is to find $\{\lambda_{A1}, \lambda_{A2}, \lambda_{B1}, \lambda_{B2}, \lambda_{C1}, \lambda_{C2}\}$ such that:

$$\begin{bmatrix} d_{1D} & 1 \\ \dots & \dots \\ d_{ND} & 1 \end{bmatrix} = \mathbf{a} \begin{bmatrix} \lambda_{A1} & 0 \\ 0 & \lambda_{A2} \end{bmatrix} = \begin{bmatrix} \alpha_1 & \beta \\ \dots & \dots \\ \alpha_N & \beta \end{bmatrix} \begin{bmatrix} \lambda_{A1} & 0 \\ 0 & \lambda_{A2} \end{bmatrix} \quad \text{Eq. 8}$$

$$\begin{bmatrix} 1 & d_{1D} \\ \dots & \dots \\ 1 & d_{ND} \end{bmatrix} = \mathbf{b} \begin{bmatrix} \lambda_{B1} & 0 \\ 0 & \lambda_{B2} \end{bmatrix} = \begin{bmatrix} \gamma & \delta_1 \\ \dots & \dots \\ \gamma & \delta_N \end{bmatrix} \begin{bmatrix} \lambda_{B1} & 0 \\ 0 & \lambda_{B2} \end{bmatrix} \quad \text{Eq. 9}$$

$$\frac{2\pi f_s}{vK} \begin{bmatrix} k_0 - k_0 & k_0 - k_0 \\ \dots & \dots \\ k_M - k_0 & k_M - k_0 \end{bmatrix} = \mathbf{c} \begin{bmatrix} \lambda_{C1} & 0 \\ 0 & \lambda_{C2} \end{bmatrix} = \begin{bmatrix} \mu_1 & \epsilon_1 \\ \dots & \dots \\ \mu_K & \epsilon_K \end{bmatrix} \begin{bmatrix} \lambda_{C1} & 0 \\ 0 & \lambda_{C2} \end{bmatrix} \quad \text{Eq. 10}$$

satisfying the followings constraints [5]:

$$\begin{cases} \lambda_{A1}\lambda_{B1}\lambda_{C1} = 1 \\ \lambda_{A2}\lambda_{B2}\lambda_{C2} = 1 \end{cases} \quad \text{Eq. 11}$$

By analyzing the above equations, it can be easily seen that these coefficients can be estimated as:

$$\begin{aligned} \lambda_{A2} &= 1/\beta & \lambda_{C1} &= \text{mean} \left[\frac{2\pi f_s(k - k_0)}{Kv\mu_k} \right] & \lambda_{A1} &= \frac{1}{\lambda_{B1}\lambda_{C1}} \\ \lambda_{B1} &= 1/\gamma & \lambda_{C2} &= \text{mean} \left[\frac{2\pi f_s(k - k_0)}{Kv\epsilon_k} \right] & \lambda_{B2} &= \frac{1}{\lambda_{A2}\lambda_{C2}} \end{aligned} \quad \text{Eq. 12}$$

It is important here to notice that to go back from an arbitrary numerical CPD to a CPD that is physically relevant, the knowledge of the velocity v is needed. This descaling factor, *i.e.* the velocity of Lamb waves within the material is here indeed necessary to convert a time-domain information (extracted from phase here) to a distance information as done in any classical localization algorithm [12, 13, 11]. However, the Lamb wave velocity v can be very easily estimated from experimental data in the reference state by computing the times of arrivals of the first wave packets and making use of the known distances between piezoelectric elements.

In summary, it is shown here that starting from a numerical CPD of the phase tensor and using knowledge on the velocity v of Lamb waves within the material under study derived from input experimental data, it is possible to access to two estimates of the distances between all the piezoelectric elements and the damage $\{d_{iD}^a\}_{i \in [1, N]}$ and $\{d_{iD}^b\}_{i \in [1, N]}$.

Even if theoretically $\forall i \in [1, N] \ d_{iD}^a = d_{iD}^b$, this may not be the case in practice due to several factors (experimental noise, numerical issues, ...) and it has thus been chosen to introduce and to keep the two notations.

2.4. Damage localization imaging

The last step of the damage localization algorithm consists now in drawing a map able to highlight the most probable damage localization from the two sets of distances $\{d_{iD}^a\}_{i \in [1, N]}$ and $\{d_{iD}^b\}_{i \in [1, N]}$ estimated previously. Let's consider a structure under study over which coordinates of a current point P can be defined. It is then possible to compute for any current point on the structure the distances $\{d_{iP}\}_{i \in [1, N]}$ between this current point and the N piezoelectric elements. The point of the structure that will most probably be the damage location should thus in theory satisfy:

$$\forall i \in [1, N] \ d_{iP} = d_{iD}^a = d_{iD}^b \quad \text{Eq. 13}$$

Consequently, a very intuitive damage localization index (DLI) can be defined as:

$$\text{DLI}(P) = \frac{1}{\sum_{i=1}^N (2d_{iP} - d_{iD}^a - d_{iD}^b)^2} \quad \text{Eq. 14}$$

Finally, the damage imaging algorithm simply consists in plotting $\text{DLI}(P)$ over the structure and in searching for its maximum value. One can notice that the choice done here is arbitrary and that other potentially more optimal choices could have been made (minimizing the sum of squares, separate optimization procedures using d_{iD}^a and d_{iD}^b , ...).

2.5. Algorithm overview

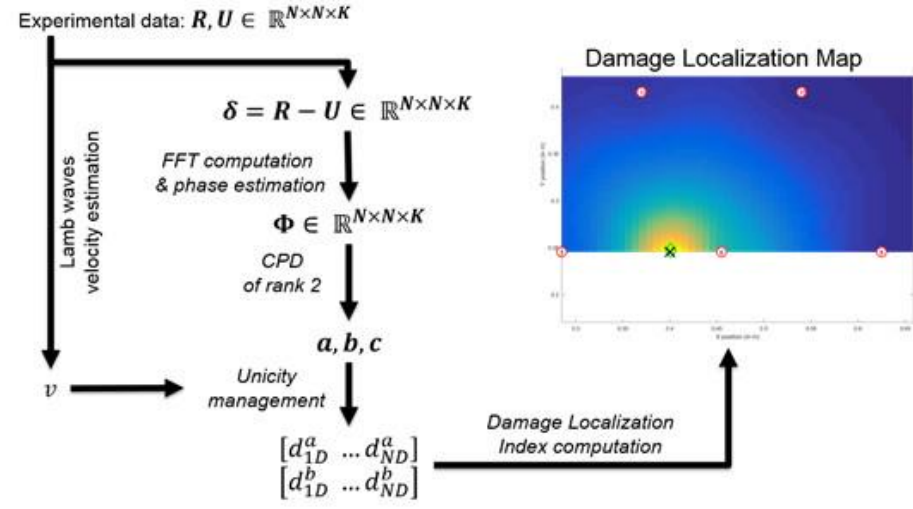


Fig. 2: Overview of the damage localization algorithm

The damage localization algorithm proposed here can thus be summarized as follows:

- Step 1: Compute the difference tensor δ between a reference and an unknown state.
- Step 2: Compute the phase of the Fourier transform for the difference signal on the path “actuator n – sensor m ” and build the tensor Φ on this basis (see Sec. 2.1).
- Step 3: Compute the CPD of rank $R = 2$ of the tensor Φ (see Sec. 2.2).

- *Step 4:* Estimate Lamb wave velocity v to descale the previous numerically obtained CPD and extract damage to piezoelectric elements distances estimates $\{d_{iD}^a\}_{i \in [1,N]}$ and $\{d_{iD}^b\}_{i \in [1,N]}$ (see Sec. 2.3).
- *Step 5:* Compute the damage localization index and draw a damage localization map in order to estimate the most probable damage localization (see Sec. 2.4).

3. Experimental results

3.1. Experimental setup

The geometrically complex aeronautics structure under study consists here in the fan cowl part of a nacelle of an Airbus A380. This structure is 1.5 m in height for a semi circumference of 4 m and is made of composite monolithic carbon epoxy material. It has been equipped with 30 piezoelectric elements manufactured by NOLIAAC (diameter of 25 mm) and possesses many stiffeners delimiting various areas; as shown in Figure 3. This part is particularly challenging because it contains several stiffeners. The damage is simulated using two 35 mm Neodymium magnets placed on both faces of the structure at the position indicated by the yellow “X”.

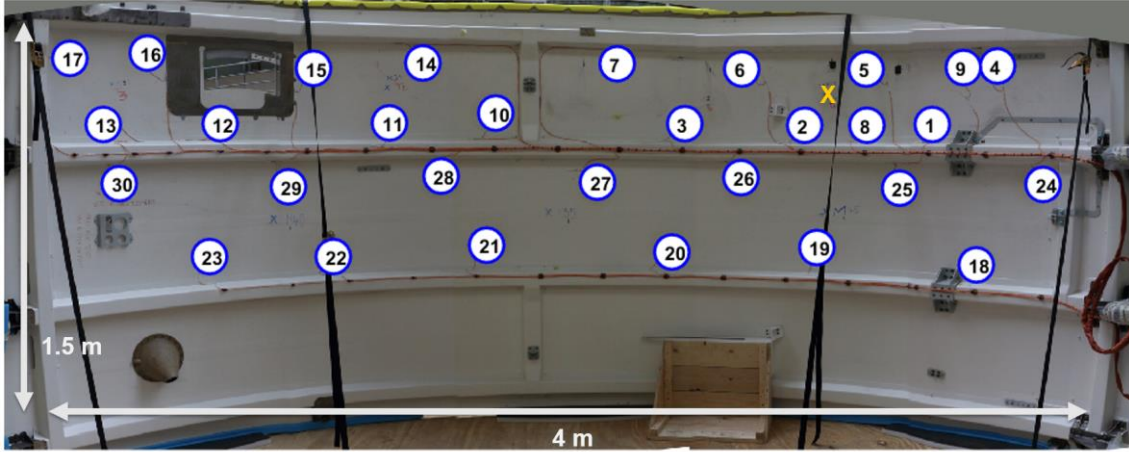


Figure 3: Fan cowl of an A380 Nacelle made of composite materials and equipped with 30 piezoelectric elements and possessing many stiffeners. Damage position is indicated with the yellow “X”.

The excitation signal sent to the PZT element is a “5 cycles burst” with a central frequency of $f_0 = 200$ kHz and with an amplitude of 10 V. This signal has been chosen here to maximize the propagation of the S_0 mode [11, 12]. In each phase of the experimental procedure, one PZT is selected as the actuator and the other act as sensors. All the PZTs act sequentially as actuators. Resulting signals are then simultaneously recorded by the others piezoelectric element and consist of 1500 data points sampled at 1 MHz. The Lamb wave propagation speed within the material is estimated around 5200 m/s for the S_0 mode. Signals were acquired 10 times in both the healthy (reference) and damaged (unknown) states.

As pre-processing steps, the measured signals are first denoised by means of a discrete wavelet transform up to the order 4 using the “db40” wavelet. Those signals are then filtered around their center frequency f_0 using a continuous wavelet transformation based on “morlet” wavelets and with a scale resolution equals to 20. The diaphonic part present in the measured signals (*i.e.* the copy of the input signals that appears on the measured signal due to electromagnetic coupling in wires) has been previously eliminated based on

the knowledge of the geometrical positions of the PZT and of the estimated waves propagation speed v in the material.

3.2. CPD of the phase tensor in practice

To build the tensors Φ and \mathbf{A} (see Sec. 2.1), the matrix δ containing the differences of signals between the healthy and damaged states have been built. To remove undesirable reflections from the differences signals, only the first wave packets have been retained in the difference signals. In Figure 4 [Left], the resulting normalized pre-processed difference signals are plotted in blue as well as the corresponding input signals (in red). From this figure it can be seen that the simplified underlying hypothesis leading to Eq. 3 is well satisfied after the pre-processing steps (denoising and first wave packet isolation): indeed, the difference signals contain a single reflection that arrive to sensor with variable delays. It should also be noted that in practice due to the data acquisition system being used, the piezoelectric elements can be considered either as actuators or as sensors, but not as both. Thus, nothing is measured on the “diagonal” part of the tensor (*i.e.* when $n = m$, see the diagonal of Figure 4). In practice the matrices δ and Φ are thus only partially known.

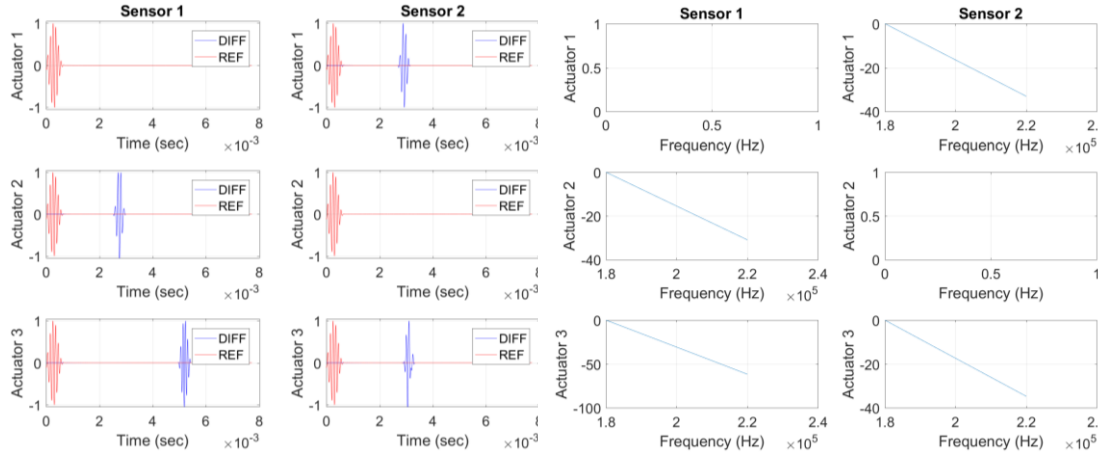


Figure 4: [Left] Example of input signals (red) and of pre-processed difference signals (blue) for several “actuator-sensor” paths. Amplitudes have been normalized. [Right] Part of the phase tensor Φ for several “actuator-sensor” paths. Phase is plotted in the range $[0.9f_0, 1.1f_0]$ with $f_0 = 200$ kHz.

The phase and amplitude are then computed from the discrete Fourier transform of these signals. As input signals are band limited around their central frequency f_0 , only the phase and amplitude in the range $[0.9f_0, 1.1f_0]$ is considered here. The phases, which are parts of the phase tensor Φ are plotted in Figure 4 [Right]. From this figure as expected from Eq. 5, the phases decrease linearly with the frequency and the slopes of these phases are different.

The next step consists in computing first numerical CPDs of the phase and amplitude tensors. These CPDs are computed using the TensorLab toolbox running in a Matlab environment [14]. Obtaining a numerical CPD is nothing else than solving an optimization problem satisfying some constraints associated with the particular form of the decomposition being sought. Thus, initial values of the triplets ($\mathbf{a} \in \mathbb{R}^{N \times R}$, $\mathbf{b} \in \mathbb{R}^{N \times R}$, $\mathbf{c} \in \mathbb{R}^{K \times R}$) must be provided to the optimization algorithm before running it. Here \mathbf{c} is initialized according to Eq. 7 as information regarding Lamb waves velocity v has

been previously estimated. The matrices \mathbf{a} and \mathbf{b} are initialized by considering that an initial guess localization for the damage is the barycenter of all the positions of the piezoelectric elements. The CPDs are then obtained through a nonlinear least squares algorithm. Once the two numerical CPDs are obtained, they are descaled to allow for their physical interpretation as explained in Sec. 2.3. At that moment it is then possible to access to two estimates of the distances between all the piezoelectric elements and the damage $\{d_{iD}^a\}_{i \in [1,N]}$, and $\{d_{iD}^b\}_{i \in [1,N]}$ (see Sec. 2.3) and to compute the damage localization index defined by Eq. 14 for all points M in the area of interest where the damage could be located. As for each case under study 10 repetitions in the healthy and damaged states are available, the damage localization index is computed 100 times.

3.3. Localization results

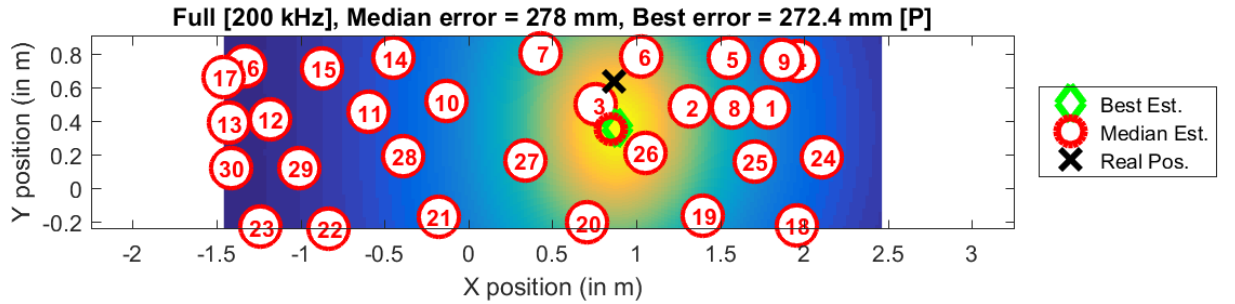


Figure 5: Obtained localization results for the different damage localization indexes and for the full structure under study.

Localization results are provided in Figure 5. On this figure, the damage localization index is plotted for the case under study as well as the positions of the different piezoelectric elements. In addition to the resulting damage localization maps, the position of the actual damage as well as the position of the best estimation and of the median estimation provided by the algorithm are provided. Furthermore, the associated “*Best errors*” and “*Median errors*” are reported in the title and are both around 27 cm. The median estimated localization for each case under study lies relatively close to the actual damage position when considering the overall structure dimension. It can also be seen that the damage localization maps provided by the damage localization index graphically indicate the correct area and that the best localization results are really close to the actual damage position. Thus, the relative localization error (i.e. the localization error divided by the larger portion of the structure expressed in %) is $\simeq 6 - 7\%$ for the case being considered. Another noticeable point with respect to the proposed algorithm is that it takes as inputs directly the signals measured by all the piezoelectric elements without any additional preprocessing or selection steps. This makes the algorithm relatively robust in the present case.

4. CONCLUSION

Monitoring in real-time and autonomously the health state of aeronautic structures is referred to as Structural Health Monitoring (SHM) and is a process decomposed in four steps: damage detection, localization, classification, and quantification. Structure under study was here a complex aeronautic nacelle and the focus was put on the localization step of the SHM process. The fact that SHM data are naturally three-way tensors has been investigated for this purpose. It is demonstrated in this paper that under classical assumptions regarding wave propagation, the canonical polyadic decomposition of rank

2 of the tensor built from the phase of the difference signals between a healthy and damaged states provides direct access to the distances between the piezoelectric elements and the damage. This property is used here to propose an original and robust tensor-based damage localization algorithm. This algorithm is successfully validated on experimental data coming from the structure under study. Thanks to the tensor formalism this algorithm appears to be very robust when integrating all the information together in the localization process through the canonical polyadic decomposition. Future work will now focus on a methodological comparison between this tensor-based algorithm and classical algorithms thanks to numerical simulations and experimental data.

5. REFERENCES

- [1] D. Balageas, C.-P. Fritzen et A. Güemes, Structural health monitoring, vol. 493, Wiley Online Library, 2006.
- [2] C. R. Farrar et K. Worden, «An introduction to structural health monitoring,» *Philosophical Transactions of the Royal Society of London A: Mathematical, Physical and Engineering Sciences*, vol. 365, pp. 303-315, 2007.
- [3] K. Worden, C. R. Farrar, G. Manson et G. Park, «The fundamental axioms of structural health monitoring,» *Proceedings of the Royal Society of London A: Mathematical, Physical and Engineering Sciences*, vol. 463, pp. 1639-1664, 2007.
- [4] T. G. Kolda et B. W. Bader, «Tensor decompositions and applications,» *SIAM review*, vol. 51, pp. 455-500, 2009.
- [5] N. D. Sidiropoulos, L. De Lathauwer, X. Fu, K. Huang, E. E. Papalexakis et C. Faloutsos, «Tensor decomposition for signal processing and machine learning,» *IEEE Transactions on Signal Processing*, vol. 65, pp. 3551-3582, 2017.
- [6] H. Fanaee-T et J. Gama, «Tensor-based anomaly detection: An interdisciplinary survey,» *Knowledge-Based Systems*, vol. 98, pp. 130-147, 2016.
- [7] P. Cheema, N. L. D. Khoa, M. Makki Alamdari, W. Liu, Y. Wang, F. Chen et P. Runcie, «On Structural Health Monitoring Using Tensor Analysis and Support Vector Machine with Artificial Negative Data,» chez *Proceedings of the 25th ACM International on Conference on Information and Knowledge Management*, 2016.
- [8] M. A. Prada, J. Toivola, J. Kullaa et J. Hollmén, «Three-way analysis of structural health monitoring data,» *Neurocomputing*, vol. 80, pp. 119-128, 2012.
- [9] R. You, Y. Yao et J. Shi, «Tensor-based ultrasonic data analysis for defect detection in fiber reinforced polymer (FRP) composites,» *Chemometrics and Intelligent Laboratory Systems*, vol. 163, pp. 24-30, 2017.
- [10] R. Zheng, K. Nakano, R. Ohashi, Y. Okabe, M. Shimazaki, H. Nakamura et Q. Wu, «PARAFAC Decomposition for Ultrasonic Wave Sensing of Fiber Bragg Grating Sensors: Procedure and Evaluation,» *Sensors*, vol. 15, pp. 16388-16411, 2015.
- [11] Z. Su et L. Ye, Identification of damage using Lamb waves: from fundamentals to applications, vol. 48, Springer Science & Business Media, 2009.
- [12] C. Fendzi, N. Mechbal, M. Rebillat, M. Guskov et G. Coffignal, «A general Bayesian framework for ellipse-based and hyperbola-based damage localization in anisotropic composite plates,» *Journal of Intelligent Material Systems and Structures*, vol. 27, pp. 350-374, 2016.
- [13] C. Fendzi, M. Rebillat, N. Mechbal, M. Guskov et G. Coffignal, «A data-driven temperature compensation approach for Structural Health Monitoring using Lamb waves,» *Structural Health Monitoring*, vol. 15, pp. 525-540, 2016.
- [14] N. Vervliet, O. Debals, L. Sorber, M. Van Barel et L. De Lathauwer, «Tensorlab 3.0,» 2016.